

In-Plane Plasmonic Modes in a Quasicrystalline Array of Metal Nanoparticles

Zi-Lan Deng · Zhao-Hong Li · Jian-Wen Dong ·
He-Zhou Wang

Received: 12 December 2010 / Accepted: 22 March 2011
© Springer Science+Business Media, LLC 2011

Abstract We investigated the plasmonic modes in a two-dimensional quasicrystalline array of metal nanoparticles. The polarization of the modes is in the array plane. A simplified eigen-decomposition method is presented with the help of rotational symmetry. Two kinds of anti-phase ring modes with radial and tangential polarizations are of highest spatial localizations among all of plasmonic modes. For the leaky characteristic of the anti-phase ring modes, the highest fidelity mode in the quasicrystalline array is found to be tangential polarized mode, whereas normal-to-plane polarized mode in the circular ring. The leaky characteristics and spatial localizations of other plasmonic modes are also studied, for example, collective vortex mode that may be a candidate to form negative responses in plasmonic device and collective radial mode that may be used to generate light sources with radial polarizations.

Keywords Surface plasmon polariton · Metal nanoparticle · Quasicrystal · Localization

Introduction

Plasmonic materials have been paid tremendous attentions due to the significant improvement in fabrication techniques [1, 2] and their practical applications. The subwave-

length phenomena and strong near-field enhancement near optical frequencies [3, 4] enable us to use plasmonic materials as building blocks for a variety of nanoscale optical applications [5], such as biosensors [6, 7], sub-wavelength waveguides [8, 9], optical left-handed meta-materials [10], plasmonic and hybrid waveguides [11, 12], invisibility [13], beam splitter [14], and even plasmonic sources [15].

Besides applications, plasmonic systems are interested because the underlying physics is somewhere in between electronic and photonic system but has unique academic interest [16–21]. The electronic system has true eigenmodes derived from bound states. The localization is entirely concerned with the spatial localization of the electronic wavefunctions [22–24]. For two-dimensional (2D) dielectric photonic systems, it also has true eigenstates derived from scattering states. The localization is still an essential study of spatial properties in real space eigenmodes [23, 24]. Although plasmonic systems are intrinsic long range in coupling similar to photonic crystal, the resonances bear resemblance to the electronic bound states, more than to the photonic scattering states. For two-dimensional plasmonic system, it has radiation loss and thus we are dealing with quasi-eigenmodes. An extra dimension should be added in order to describe the fidelity or the radiation loss of the localized modes. Thus, we are dealing with the localization properties of “leaky” states with long-range couplings in an open system.

Up to now, Anderson localization of plasmonic eigenmodes in random arrays [19–21], as well as leaky wave of quasicrystalline structures [18, 25], has been studied. The physics is anticipated to be richer and more complicated than those in electronic and photonic systems. In this paper, the characteristics of plasmonic modes with the polarization in the array plane, i.e., in-plane (IP) modes, are investigated

Z.-L. Deng · Z.-H. Li · J.-W. Dong (✉) · H.-Z. Wang (✉)
State Key Laboratory of Optoelectronic Materials and
Technologies, Sun Yat-Sen (Zhongshan) University,
Guangzhou 510275, China
e-mail: dongjwen@mail.sysu.edu.cn

H.-Z. Wang
e-mail: stswhz@mail.sysu.edu.cn

with the help of rotational symmetry analysis and eigen-decomposition (ED) method. Compared with the normal-to-plane (NP) modes studied previously [25], the IP modes are more complicated. The polarization of the NP modes is perpendicular to the array plane, and thus the dipole moment of each particle is a scalar. For the IP modes, the polarized direction is inside the array plane, and the dipole moment can point to any direction in a 2D Cartesian coordinate. So, the dipole moments should be a vector with two components. The fact that the eigenvector is not a scalar but a two-component vector will lead the analysis method for the in-plane mode become more complicated than that of the normal-to-plane mode, especially when the array size is large. Simplified method should be introduced to investigate the electromagnetic (EM) localization characteristics. Also, the in-plane mode has its unique EM phenomena. We found that the resonant frequency spectra of radiating and weakly radiating in-plane modes are found to mix together, which is more complicated than the NP modes. The plasmonic mode with highest spatial localization and high fidelity is found to be a type of in-plane ring mode with tangential polarization, which is different from the circular ring [26]. In addition, different localized modes have very different radial decay behaviors and there is no special relationship between the fidelity of the modes and their spatial localization.

Eigen-decomposition Method in Quasicrystalline System

The plasmonic system under study is a metal nanoparticles (MNP) array arranged as 2D quasicrystal (QC) with 12-fold symmetry generated by the generalized dual method [27]. We assume each particle has a dynamic dipole polarizability, $\alpha = i(3/2k_0^3)a_1$, where $i = \sqrt{-1}$, $k_0 = \omega/c$, with c as the speed of light, and a_1 is the electric term of the Mie's coefficients [28]. We use Drude-type permittivity $\varepsilon(\omega) = 1 - \omega_p^2 / (\omega^2 + i\gamma\omega)$ with ω as the angular frequency, ω_p as the plasma frequency, and γ as the electron scattering rate. In order to meet the criteria of the dipole approximation, we restrict ourselves to the situations when the particles are not too close together with a condition of $a_{\min} \geq 3r_0$, where a_{\min} is the distance between two nearest particles and r_0 is the radius of the particle. Here, we set $\omega_p = 6.18$ eV, $a_{\min} = 75$ nm, $r_0 = 25$ nm, and $\gamma = 0$.

Consider the QC array has N particles. We assume that an external time-harmonic driving electric field $E_m^{ext}e^{-i\omega t}$ acts on the m th particle located at \mathbf{R}_m , and the coupled dipole equations can be written as the form,

$$\alpha^{-1}\mathbf{p}_m - \sum_{m' \neq m} \vec{\mathbf{W}}(\mathbf{R}_m - \mathbf{R}_{m'})\mathbf{p}_{m'} = \mathbf{E}_m^{ext}, \quad (1)$$

where $\mathbf{p}_m \equiv (\mathbf{p}_m, \mathbf{p}_{\parallel}, p_{m,z})$ is the m th dipole moment and $\vec{\mathbf{W}}(\cdot)$ is the dynamic Green's function. Equation 1 can be written in a matrix form as $\mathbf{Mp} = \mathbf{E}$, where $M = \alpha^{-1}I - \sum \vec{\mathbf{W}}$. For a 2D system, because the NP and IP polarization is orthogonal, the matrix can be decomposed. As a result, we can divide the equation as $\mathbf{M}_{\parallel}\mathbf{p}_{\parallel} = \mathbf{E}_{\parallel}$ for IP modes and $\mathbf{M}_{zz}\mathbf{p}_z = \mathbf{E}_z$ for NP modes. Here, $\mathbf{E} \equiv (\mathbf{E}_{\parallel}, \mathbf{E}_z)$. The size of \mathbf{M}_{\parallel} and \mathbf{M}_{zz} is $2N \times 2N$ and $N \times N$, respectively. We apply the ED method [16, 17] to analyze the electromagnetic resonances of such a plasmonic system. This method is more efficient than the previous ones that need either numerical complex root searching [29] or root approximation [30] in complex plane. In ED method, the eigenpolarizability with the form of $\alpha_{\text{eig}} = 1/\lambda$ can be well defined, where λ is the complex eigenvalues of the matrix \mathbf{M} . This quantity enables us to describe the collective resonance strength of the whole system for an external electric field pattern that is proportional to the corresponding eigenmode. Moreover, the participation ratio (PR) with the form of $P_n = \left(\sum_{m=1}^N |\hat{p}_m^{(n)}|^2 \right)^2 / \left(\sum_{m=1}^N |\hat{p}_m^{(n)}|^4 \right)$ is a good indicator to measure the order of the spatial localization of the modes, where $\hat{p}_m^{(n)}$ is the n th complex eigenvectors of the matrix \mathbf{M} . The smaller value of P_n , the higher spatial localization [25]. Note that there are N eigenvalues (α_{eig}) and N eigenvectors (i.e., N participation ratios) for one frequency of the NP modes, while $2N$ eigenvalues and $2N$ eigenvectors (i.e., $2N$ participation ratios) for one frequency of the IP modes.

Now, we classify the eigenmodes by using rotational symmetry of the F -fold plasmonic system. To simplify the eigenvalue problem, we divide the lattice points into $M+1$ sets, where $M \equiv (N-1)/F$ and N is the total number of particles. So, each set (except the one which contains only the central point located at the origin) contains F lattice points that equidistantly lie on a single ring. Then, we transform Cartesian coordinates to polar coordinates, i.e., $\mathbf{p}' = \Omega \mathbf{p}$ where Ω is the rotational matrix. After the transform, the eigenvalue problem becomes $\mathbf{M}'\mathbf{p}' = \lambda\mathbf{p}'$, where $\mathbf{M}' = \Omega \mathbf{M} \Omega^{-1}$. Due to the rotational symmetry, \mathbf{M}' remains invariant under cyclic index transform, i.e., $\mathbf{T} \mathbf{M}' \mathbf{T}^{-1} = \mathbf{M}'$, where

$$T = \begin{pmatrix} \tilde{I} & O & O & O & O \\ O & \tilde{T} & O & O & O \\ O & O & \tilde{T} & O & O \\ O & O & O & \ddots & \vdots \\ O & O & O & \dots & \tilde{T} \end{pmatrix}, \text{ and } \tilde{\mathbf{T}} = \begin{pmatrix} O & \tilde{I} & O & O & O \\ O & O & \tilde{I} & \ddots & \vdots \\ O & O & O & \ddots & O \\ O & O & O & \ddots & \tilde{I} \\ \tilde{I} & O & O & \dots & O \end{pmatrix}, \quad (2)$$

where \tilde{I} is a 3×3 identity matrix. The eigenvector of cyclic matrix $\tilde{\mathbf{T}}$ can be written as

$$\tilde{R}_{ju}^{(J)} = c_u^{(J)} e^{i2\pi J j/F}, \quad (3)$$

where $c_u^{(J)}$ is an arbitrary constant, $J, j=1,2,\dots,F$, and $u=1,2,3$. Since \mathbf{T} is formed by combining \tilde{I} and \tilde{T} as the

block-diagonal elements, the eigenvectors of \mathbf{T} have the form of

$$\begin{cases} \left(R_{0u}^{(J)}, R_{1ju}^{(J)}, R_{2ju}^{(J)}, \dots, R_{Mju}^{(J)} \right) = \left(q_{0u}^{(J)}, q_{1u}^{(J)} e^{i2\pi Jj/F}, q_{2u}^{(J)} e^{i2\pi Jj/F}, \dots, q_{Mu}^{(J)} e^{i2\pi Jj/F} \right), & J=F \\ \left(R_{1ju}^{(J)}, R_{2ju}^{(J)}, \dots, R_{Mju}^{(J)} \right) = \left(q_{1u}^{(J)} e^{i2\pi Jj/F}, q_{2u}^{(J)} e^{i2\pi Jj/F}, \dots, q_{Mu}^{(J)} e^{i2\pi Jj/F} \right), & J \neq F \end{cases} \quad (4)$$

where $q_{ku}^{(J)}$ are arbitrary constants. Since \mathbf{M}' and \mathbf{T} commute, they possess the same eigenvectors, and

$$\begin{cases} \left(p_{0u}^{'(J,K,U)}, p_{1ju}^{'(J,K,U)}, \dots, p_{Mju}^{'(J,K,U)} \right) = \left(q_{0u}^{(J,K,U)}, q_{1u}^{(J,K,U)} e^{i2\pi Jj/F}, \dots, q_{Mu}^{(J,K,U)} e^{i2\pi Jj/F} \right), & J=F \\ \left(p_{ju}^{'(J,K,U)}, \dots, p_{Mju}^{'(J,K,U)} \right) = \left(q_{1u}^{(J,K,U)} e^{i2\pi Jj/F}, \dots, q_{Mu}^{(J,K,U)} e^{i2\pi Jj/F} \right), & J \neq F \end{cases} \quad (5)$$

where $q_{ku}^{(J,K,U)}$ are another set of arbitrary constants that is different from those in Eq. 4. Here $U=1,2,3; K, k=0,1,2,\dots, M$ for $J=F$ and $K, k=1,2,\dots,M$ for $J \neq F$. In Eqs. 3, 4, and 5, the superscripts (K, J, U) are the mode indices, and the subscripts (k, j, u) are the vector element indices. Taking Eq. 5 into $\mathbf{M}'\mathbf{p}'=\lambda\mathbf{p}'$, we obtain

$$\begin{cases} \sum_{k'=0}^M \sum_{j'=1}^F \sum_{u'=1}^3 M'_{kk'jj'u'u'} q_{k'u'}^{(J,K,U)} = \lambda^{(J,K,U)} q_{ku}^{(J,K,U)}, & J=F \\ \sum_{k'=1}^M \sum_{j'=1}^F \sum_{u'=1}^3 M'_{kk'jj'u'u'} q_{k'u'}^{(J,K,U)} e^{i2\pi Jj'/F} = \lambda^{(J,K,U)} q_{ku}^{(J,K,U)} e^{i2\pi Jj/F}, & J \neq F \end{cases} \quad (6)$$

Introducing a new matrix

$$\tilde{M}'^{(J)}_{kk'uu'} = \sum_{j'=1}^F M'_{kk'Fj'u'u'} e^{i2\pi Jj'/F} \left(u, u' = 1, 2, 3; \quad k, k' = \begin{cases} 0, 1, \dots, M \text{ for } J=F \\ 1, 2, \dots, M \text{ for } J \neq F \end{cases} \right). \quad (8)$$

The eigenvalue problem becomes $\tilde{M}'^{(J)} q^{(J)} = \lambda^{(J)} q^{(J)}$. We note that the dimension of $\tilde{M}'^{(J)}$ is $3(M+1) \times 3(M+1)$ for $J=F$, and $3M \times 3M$ for $J \neq F$. By exchanging index J to $F-J$, and j' to $F-j'$ in Eq. 8, we have $\tilde{M}'^{(F-J)} = \tilde{M}'^{(J)}$. It indicates that the eigenmodes indexed by J and $F-J$ are degenerate. For 12-fold QC system ($F=12$), the $J=1,2,3,4,5$ eigenmodes are degenerate with the $J=11,10,9,8,7$ eigenmodes, respectively; while the eigenmodes with $J=12$ (in-phase) and $J=6$ (anti-phase) are in general nondegenerate. So, there are seven kinds of modes with different rotational symmetry. In the calculations, we divide $\tilde{\mathbf{M}}'^{(J)}$ into $\tilde{\mathbf{M}}'^{(J)}_{//}$ and $\tilde{\mathbf{M}}'^{(J)}_{zz}$ in order to obtain IP and NP plasmonic modes, respectively. We use standard numerical

thus, we can write the eigenvectors of \mathbf{M}' in the form of

$$\begin{cases} \sum_{k'=0}^M \sum_{u'=1}^3 \left(\sum_{j'=1}^F M'_{kk'Fj'u'u'} \right) q_{k'u'}^{(J,K,U)} = \lambda^{(J,K,U)} q_{ku}^{(J,K,U)}, & J=F \\ \sum_{k'=1}^M \sum_{u'=1}^3 \left(\sum_{j'=1}^F M'_{kk'Fj'u'u'} e^{i2\pi Jj'/F} \right) q_{k'u'}^{(J,K,U)} = \lambda^{(J,K,U)} q_{ku}^{(J,K,U)}, & J \neq F \end{cases} \quad (7)$$

routines in LAPACK to diagonalize $\tilde{M}'^{(J)}_{//}$ and $\tilde{M}'^{(J)}_{zz}$ for each J . With the help of the above method, the dimension of the matrix is significantly reduced so that the plasmonic modes of large sample (e.g., $N \approx 10,000$) can be solved out. This is impossible if we diagonalize the matrix \mathbf{M} directly with limited computation resources and acceptable computation time. Unfortunately, the sequence of the eigenmodes is random, and it seems hard to connect the eigenvalues from one frequency to another. Thanks to the symmetry of the QC, we use the similarity of the coefficients $q_{ku}^{(J,K,U)}$ between neighboring frequencies to connect eigenvalues readily. Note that this connection cannot be done if we diagonalize the matrix \mathbf{M} directly.

Using the above method, the matrix dimension for the NP mode can be deduced to $(M+1) \times (M+1)$ for $J=F$, and $M \times M$ for $J \neq F$. The dipole moment of each particle is a scalar. For the IP mode, the matrix dimension can be deduced to $2(M+1) \times 2(M+1)$ for $J=F$, and $2M \times 2M$ for $J \neq F$. The dipole moments should be a vector with two components. So, we can reduce the matrix size significantly and investigate a cluster with larger number of particles. Furthermore, when the lattice size becomes larger and larger, the eigenstates will be overwhelming. In Ref. [25], we can only employ colors to mark the different frequency regions. In this paper, we can connect points into curves so that we can classify the modes by mode index (see below discussion and the result of Fig. 1). In this way, the physical picture becomes clearer, and the analysis of the mode properties is available, even for the large array size. In addition, the proposed method is not only available to the 2D cluster arranged as 12-fold QC but also useful and efficient for any other cluster possessing rotational symmetry, such as eightfold and 20-fold QC, concentrically circular array, and so on.

Results and Discussions

Figure 1 shows an intensity plot of $\text{Im}(\alpha_{\text{eig}})$ on the plane of frequency and mode index in the 12-fold QC with $N=1,513$. Here, we use the symbol m instead of (K, U) to represent the mode index. Figure 1a, b shows the cases of the anti-phase ($J=6$) NP and in-phase ($J=12$) NP modes;

while Fig. 1c, d shows the cases of the anti-phase IP and in-phase IP modes, respectively. Here, we only show the results of $J=6$ and $J=12$ since the modes with other J indices are quite similar. As a spectral function, the peaks of $\text{Im}(\alpha_{\text{eig}})$ represent resonances. The mode index, m , is used to identify the mode whose resonant frequency is sorted in an increasing order. In fact, $\text{Im}(\alpha_{\text{eig}})$ is proportional to the extinction of the driving field, and the width of the peak in the spectra shows automatically the mode quality (fidelity). The larger the peak width is, the less dramatic color changes and the stronger radiating the mode is. It can be seen, for the NP modes, that the spectral function has narrow and conspicuous peaks near 3.25 eV, while large and smooth peaks located in lower and higher frequency ranges. It indicates that the modes with weakly out-of-plane radiating loss are separated from the radiating modes at both sides. This is consistent with our previous findings [25]. But this explicit characteristic is not found in the spectra of IP modes. It can be seen, from Fig. 1c, d that the radiating and weakly radiating modes are mixed together in the frequency range.

In Ref. [25], we introduced a trajectory map in a three-dimensional parameter space $(\omega, |\lambda|, P_n)$, which can give information about the temporal properties and the spatial properties of the modes. In this paper, we follow the idea but use a more simple representation. We pick out the resonant frequency for each mode and dot it in a two-dimensional parameter space [$\text{Im}(\alpha_{\text{eig}}), P_n$]. Figure 2 shows the results for different kinds of anti-phase IP plasmonic modes in different sizes of the MNP clusters.

Fig. 1 Intensity plot of $\log_{10} [\text{Im}(\alpha_{\text{eig}})]$ for the resonant spectra of plasmonic eigenmodes with a 12-fold quasicrystal; **a** and **b** for the anti-phase and in-phase normal-to-plane modes, while **c** and **d** for the anti-phase and in-phase in-plane modes, respectively (color online)

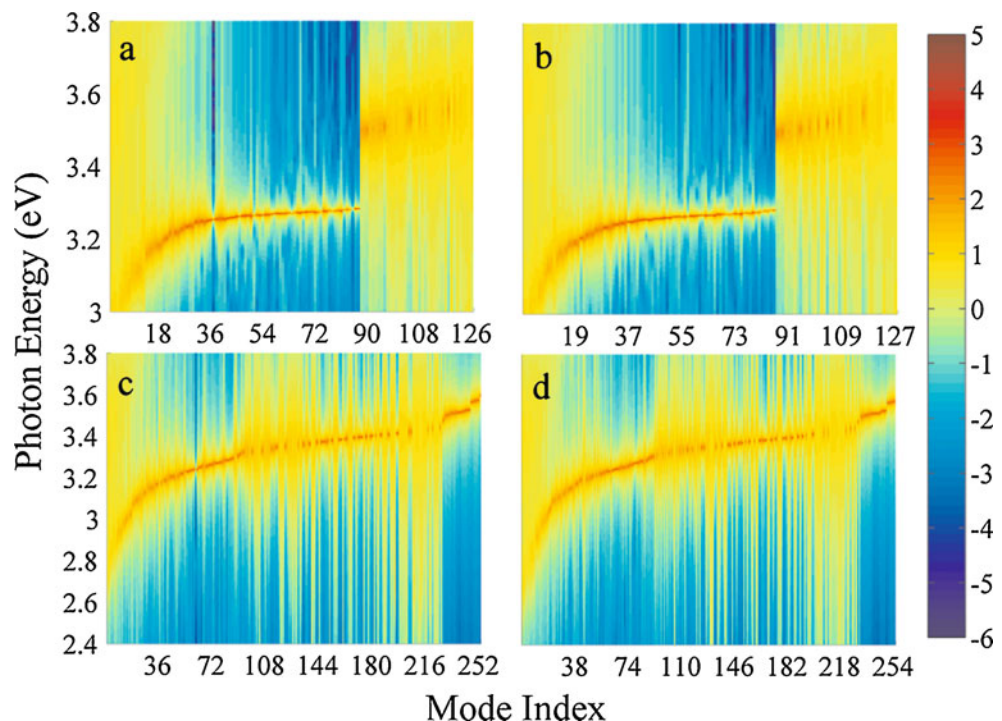
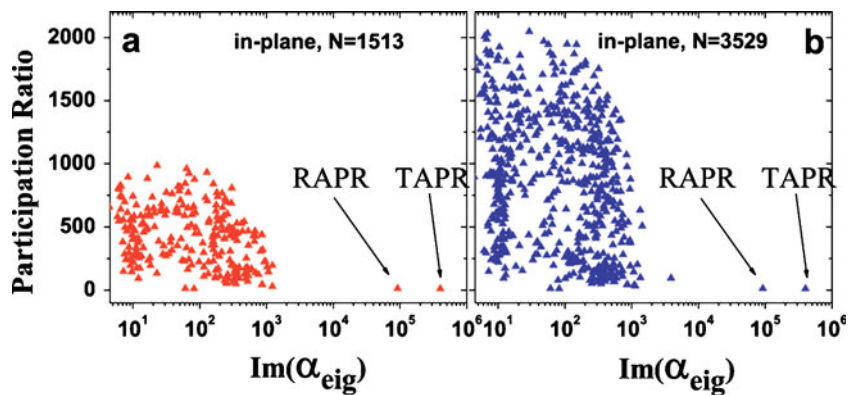


Fig. 2 Participation ratio vs. $\text{Im}(\alpha_{\text{eig}})$ at resonant frequency for the anti-phase in-plane modes with different numbers of particles. The particle number of the cluster is 1,513 and 3,529, respectively (color online)



On one hand, there are localized modes, whose PR values are much smaller than the cluster number, and they almost remain the same when the size of the cluster increases. On

the other hand, there are also extended modes whose PR values are expanded to approximately twice when the particles of the cluster increase from 1,513 to 3,529.

Fig. 3 Characteristics of three anti-phase ring modes with different number of particles. The dipole distributions for the **a** RAPR, **b** TAPR, and **d** NAPR mode. The directions and lengths of arrows represent polarization directions and magnitudes, and the red/blue color represents positive/negative maximum. **d** The resonant frequency, **e** the PR value, and **f** $\text{Im}(\alpha_{\text{eig}})$ as the function of the number of particles (color online)

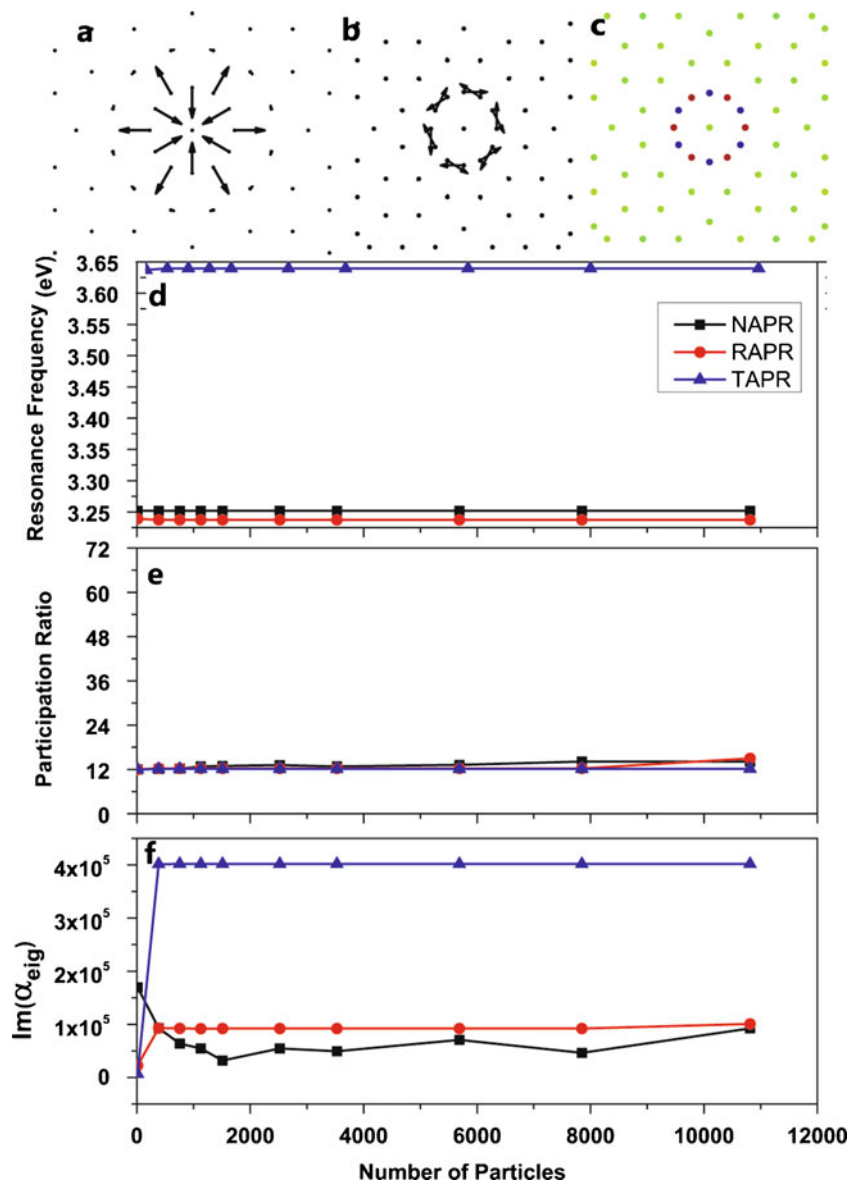


Fig. 4 The dipole distributions of other different type of localized modes. **a** In-phase ring in-plane mode, **b** in-plane large ring mode, **c** collective vortex mode, and **d** collective radial mode. The number of particles of the cluster is $N=1,513$

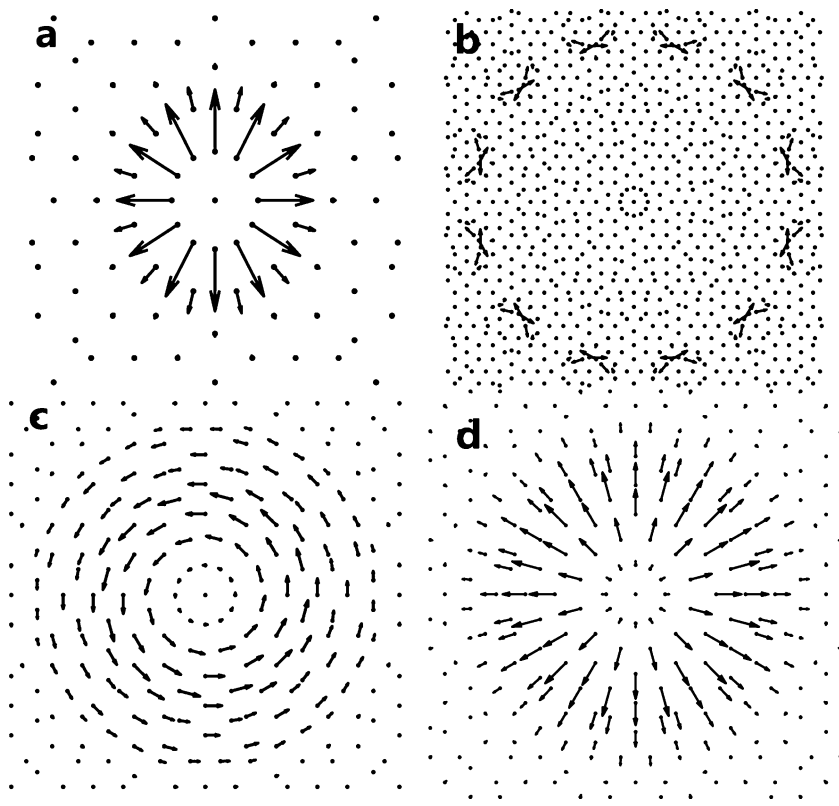
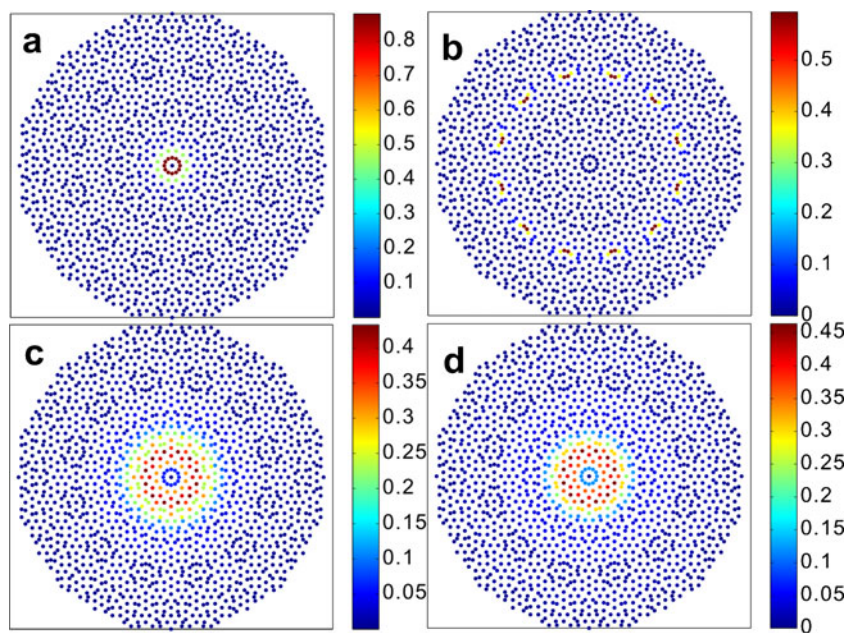


Figure 2 also shows that there is no special relationship between the radiation (fidelity) of the modes and their spatial localization. What is more, it is interesting to find that there are two anti-phase IP modes with the largest $\text{Im}(\alpha_{\text{eig}})$ and the smallest PR in the bottom right of Fig. 2a, b. It indicates that they are highest spatially localized and have highest fidelity. As discussed below, these two IP modes are

the radial anti-phase ring (RAPR) mode and the tangential anti-phase ring (TAPR) mode.

Next, we will turn to focus on two anti-phase ring modes. Figure 3a, b shows the mode patterns (dipole moment distribution) of RAPR and TAPR modes, respectively. In order to compare with the ring mode whose dipole moment directions point to normal-to-plane, we also plot

Fig. 5 The electric field magnitude distributions of the corresponding in-plane plasmonic modes shown in Fig. 4 (color online)



the mode pattern of normal anti-phase ring (NAPR) mode in Fig. 3c. Because the dipole moments of these three ring modes are strongly confined on the central ring of the QC, we just show the dipole moments near the center. The magnitude of the dipole is exactly the same in every particle within the central ring. But the direction of the dipole is different from each mode. It is along radial direction of array plane for the RAPR mode, along tangential direction of array plane for the TAPR mode, and perpendicular to the array plane for the NAPR mode. In addition, no matter which anti-phase ring mode in Fig. 3a–c, the direction of the neighboring dipoles are opposite in sign. As shown in Fig. 2, we find that the anti-phase ring modes are highest spatially localized and have highest fidelity. In order to give more evidence, we have calculated for larger size of clusters, and the results are shown in Fig. 3d–f. It is found that the resonant frequency and the PR value are almost unchanged even when the number of particles reaches over 10,000. It indicates that the anti-phase ring modes are indeed well-defined localized modes. Moreover, the resonant frequencies of both NAPR and RAPR are near the resonant frequency of a single particle (3.25 eV), while the resonant frequency of TAPR (3.63 eV) is largely above that of a single particle (see Fig. 3d). This is analogous to the ring modes in a circular array [26]. Figure 3f shows that the NAPR mode has the highest fidelity when the cluster has only a ring pattern ($N=13$), which is in accordance with Ref. [26]. However, when the cluster arranges into the QC shape, simulation results show that the mode with highest fidelity is the TAPR mode instead of the NAPR mode. Note that the above anti-phase ring mode cannot be excited by the plane wave. But it can be still excited if we use an appropriate incident wave, e.g., the dipole antenna with appropriate frequency and direction placed near the particles of the inner ring.

Apart from the anti-phase ring modes, there are many other different localized modes. For example, there is a kind of in-phase ring IP mode, of which the energy is concentrated on the inner two rings near the center point (see Figs. 4a and 5a). All dipoles are radially polarized and in-phase (see Fig. 4a). From its Fourier spectrum, it is found that the in-phase IP mode is strong radiating and has low mode quality due to the boundary match to free space. There is another typical localized mode with threefold rotational symmetry, whose dipolar pattern is shown in Fig. 4b and electric field magnitude distributions is shown in Fig. 5b. The dipole moments concentrate on a large ring of the QC. The PR value of such large ring mode is about 42, much smaller than the particle number 1,513. In addition, we find many plasmonic modes with collective vortex patterns and collective radial patterns. Two representative examples are shown: vortex patterns in Figs. 4c and 5c, while radial patterns in Figs. 4d and 5d. From the electric

field magnitude distribution (Fig. 5c, d), we can see that most of the energy of these modes is localized in the central area of QC array. The dipole moment are in phase but the vector's direction is azimuthal and radial, respectively (Fig. 4c and 4d). The vortex mode is promising to induce a large magnetic field so that it may be a candidate to form negative response and plasmonic metamaterials. However, the size of the vortex mode is larger than the resonant wavelength, so effective medium theory will fail to employ and effective refractive indexes is meaningless. The effective refractive indexes may be calculated from a QC cluster with smaller size particles. In addition, the radial mode may be potentially used to produce light sources with radial polarizations [31].

Summary

In summary, we have investigated the rotational symmetry, the radiating properties, and the spatial localization properties of in-plane plasmonic eigenmodes in the QC MNP lattice. A simplified form of the eigen-problem has been derived so that the overwhelming information in the large system can be reduced according to the symmetry of the QC. Two anti-phase ring modes with different polarizations are found to be of high fidelity and high spatial localization. In particular, the anti-phase ring mode with tangential polarization has the highest fidelity. Other localized mode and the collective vortex and collective radial mode are also studied.

Acknowledgments We would like to thank Prof. C. T. Chan for his valuable discussions. This work is supported by the National Natural Science Foundation of China (10804131, 11074311, 10874250), the Fundamental Research Funds for the Central Universities (2009300003161450), and the Guangdong Natural Science Foundation (10451027501005073).

References

1. Kreibig U, Vollmer M (1995) Optical properties of metal clusters. Springer, Berlin
2. Feldheim DL, Foss CA Jr (2002) Metal nanoparticles: synthesis, characterization and applications. Marcel Dekker, New York
3. Barnes WL, Dereux A, Ebbesen TW (2003) Surface plasmon subwavelength optics. *Nature* 424(6950):824–830
4. Girard C (2005) Near fields in nanostructures. *Rep Prog Phys* 68 (8):1883
5. Ozbay E (2006) Plasmonics: merging photonics and electronics at nanoscale dimensions. *Science* 311(5758):189–193
6. Haes AJ, Duyne RPV (2004) A unified view of propagating and localized surface plasmon resonance biosensors. *Anal Bioanal Chem* 379(7):920–930
7. Elghanian R, Storhoff JJ, Mucic RC, Letsinger RL, Mirkin CA (1997) Selective colorimetric detection of polynucleotides based

- on the distance-dependent optical properties of gold nanoparticles. *Science* 277(5329):1078–1081
8. Maier SA, Kik PG, Atwater HA, Meltzer S, Harel E, Koel BE, Requicha AAG (2003) Local detection of electromagnetic energy transport below the diffraction limit in metal nanoparticle plasmon waveguides. *Nat Mater* 2(4):229–232
 9. Quinten M, Leitner A, Krenn JR, Aussenegg FR (1998) Electromagnetic energy transport via linear chains of silver nanoparticles. *Opt Lett* 23(17):1331–1333
 10. Engheta N, Salandrino A, Alù A (2005) Circuit elements at optical frequencies: nanoinductors, nanocapacitors, and nanoresistors. *Phys Rev Lett* 95(9):095504
 11. Oulton RF, Sorger VJ, Genov DA, Pile DFP, Zhang X (2008) A hybrid plasmonic waveguide for subwavelength confinement and long-range propagation. *Nat Photonics* 2(8):496–500
 12. Krasavin AV, Zayats AV (2010) Numerical analysis of long-range surface plasmon polariton modes in nanoscale plasmonic waveguides. *Opt Lett* 35(13):2118–2120
 13. Ni Y, Gao L, Qiu CW (2010) Achieving invisibility of homogeneous cylindrically anisotropic cylinders. *Plasmonics* 5(3):251–258
 14. Lee S-Y, Park J, Woo I, Park N, Lee B (2010) Surface plasmon beam splitting by the photon tunneling through the plasmonic nanogap. *Appl Phys Lett* 97(13):133113
 15. Oulton RF, Sorger VJ, Zentgraf T, Ma RM, Gladden C, Dai L, Bartal G, Zhang X (2009) Plasmon lasers at deep subwavelength scale. *Nature* 461(7264):629–632
 16. Fung KH, Chan CT (2007) Plasmonic modes in periodic metal nanoparticle chains: a direct dynamic eigenmode analysis. *Opt Lett* 32(8):973–975
 17. Zhen YR, Fung KH, Chan CT (2008) Collective plasmonic modes in two-dimensional periodic arrays of metal nanoparticles. *Phys Rev B* 78(3):035419
 18. Micco A, Galdi V, Capolino F, DellaVilla A, Pierro V, Enoch S, Tayeb G (2009) Directive emission from defect-free dodecagonal photonic quasicrystals: a leaky wave characterization. *Phys Rev B* 79(7):075110
 19. Markel VA (2006) Anderson localization of polar eigenmodes in random planar composites. *J Phys Condens Matter* 18(49):11149
 20. Stockman MI, Faleev SV, Bergman DJ (2001) Localization versus delocalization of surface plasmons in nanosystems: can one state have both characteristics? *Phys Rev Lett* 87(16):167401
 21. Genov DA, Shalaev VM, Sarychev AK (2005) Surface plasmon excitation and correlation-induced localization-delocalization transition in semicontinuous metal films. *Phys Rev B* 72(11):113102
 22. Chan YS, Chan CT, Liu ZY (1998) Photonic band gaps in two dimensional photonic quasicrystals. *Phys Rev Lett* 80(5):956
 23. Wang YQ, Hu XY, Xu XS, Cheng BY, Zhang DZ (2003) Localized modes in defect-free dodecagonal quasiperiodic photonic crystals. *Phys Rev B* 68(16):165106
 24. Lai Y, Zhang ZQ, Chan CH, Tsang L (2006) Gap structures and wave functions of classical waves in large-sized two-dimensional quasiperiodic structures. *Phys Rev B* 74(5):054305
 25. Dong JW, Fung KH, Chan CT, Wang HZ (2009) Localization characteristics of two-dimensional quasicrystals consisting of metal nanoparticles. *Phys Rev B* 80(15):155118
 26. Fung KH, Chan CT (2008) Analytical study of the plasmonic modes of a metal nanoparticle circular array. *Phys Rev B* 77(20):205423
 27. Levine D, Steinhardt PJ (1986) Quasicrystals. I. Definition and structure. *Phys Rev B* 34(2):596
 28. Bohren CF, Huffman DR (1983) Absorption and scattering of light by small particles. Wiley, New York
 29. Weber WH, Ford GW (2004) Propagation of optical excitations by dipolar interactions in metal nanoparticle chains. *Phys Rev B* 70(12):125429
 30. Citrin DS (2005) Subwavelength nanoplasmonic ring resonators. *J Opt Soc Am B* 22(8):1763–1769
 31. Fridman M, Machavariani G, Davidson N, Friesem AA (2008) Fiber lasers generating radially and azimuthally polarized light. *Appl Phys Lett* 93(19):191104